Dispersion induced by unsteady diffusion-driven flow in parallel-plate channel

Lingyun Ding[a,b], Richard M. McLaughlin[b,*]

[a]*Department of Mathematics, University of California Los Angeles, CA, 90095, United States*
[b]*Department of Mathematics, University of North Carolina, Chapel Hill, NC, 27599, United States*

Abstract

We investigate diffusion-driven flows in a parallel-plate channel domain with linear density stratification, which arise from the combined influence of gravity and diffusion in density-stratified fluids. We compute the time-dependent diffusion-driven flows and perturbed density field using eigenfunction expansions under the Boussinesq approximation. In channel domain, the unsteady flow converges to a steady-state solution either monotonically or non-monotonically (highly oscillatory), depending on the relation between the Schmidt number and the non-dimensionalized stratified scalar diffusivity, while the flow in the half-space inclined plane problem exhibits oscillatory convergence for all parameters. To validate the Boussinesq approximation, we propose the quasi-Boussinesq approximation, which includes transverse density variation in the inertial term. Numerical solutions show that the relative difference between the Boussinesq and quasi-Boussinesq approximations is uniformly small. We also study the mixing of a passive tracer induced by the advection of the unsteady diffusion-driven flow and present the series representation of the time-dependent effective diffusion coefficient. For small Schmidt numbers, the effective diffusion coefficient induced by the unsteady flow solution can oscillate with an amplitude larger than the effective diffusion coefficient induced by the long-time-limiting steady-state flow. Interestingly, the unsteady flow solution can reduce the time-dependent effective diffusion coefficient temporally in some parameter regimes, below even that produced by pure molecular diffusion in the absence of a flow. However, at long times, the effective diffusion is significantly enhanced for large Péclet numbers.

Keywords: Stratified fluid, Low Reynolds number, Diffusion-driven flow, Passive scalar, Shear dispersion, Effective diffusion coefficient
2010 MSC: 34E13,35Q30,37A25, 37N10, 82C70, 76R50

1. Introduction

Diffusion-driven flow is a boundary layer flow that results from the combined influence of gravity and diffusion, which exists in the density-stratified fluids whenever the gravity field is

---
*Corresponding author
Email addresses: `dingly@g.ucla.edu` (Lingyun Ding), `rmm@email.unc.edu` (Richard M. McLaughlin)

not parallel to the solid boundary. The hydrostatic equilibrium in the density-stratified fluid with diffusive solute requires two conditions. First, isopycnals should be perpendicular to the direction of gravity. Second, the impermeable (i.e. no-flux) boundary condition requires that the isopycnals must always be perpendicular to an impermeable boundary to ensure that there is no diffusive flux normal to the boundary. Therefore, when the impermeable boundary is not parallel to the direction of gravity, isopycnals can not be perpendicular to both of them at the same time. The breaking of the hydrostatic equilibrium yields the diffusion-driven flow.

The diffusion-driven flow is at the same scale as molecular diffusion due to the formation mechanism, and as such could lead to interesting dynamics on long time scales or on small length scales. Therefore, the study of diffusion-driven flow historically was motivated by understanding the transport and mixing over geological time scales such as the ocean boundary mixing [28, 39] and salt transport in rock fissures [37, 20, 40, 29]. The recent applications of diffusion-driven flow have been expanded in many areas. The potential high-impact studies include the self-propulsion of immersed objects [25, 2], the molecular diffusivity measurement [1], the self-assembly of particles in a stratified fluid [7] and airflows created by mushrooms for dispersing their spores [15].

We find two points that have not been addressed well in the literature. First, the studies mentioned above mainly concern the long-time stationary configuration of the diffusion-driven flow, but little is known about the transient dynamics at the earlier stage of the diffusion-driven flow formation, which can play an important role in some parameter regimes. Kistovich et al. [21] studied the transient diffusion-driven flow induced by the inclined plane using Fourier series expansion. The series representation of the flow converges rapidly at fixed time, but suffers from non-uniformity in time as the truncations are all unbounded as time grows. Harabin [19] presented a different perspective of the same problem. He derived the flow solution valid for all time scales using the Laplace transform and demonstrate that the flow exhibits oscillatory behavior in its evolution for small Schmidt (Prandtl) numbers.

Hence, the first goal of this study is to generalize those results to tilted parallel-plate channel domain and to show how the flow properties change due to the boundary geometries. We explicitly calculate the time-dependent flow solution and the perturbed density field starting from a uniform linear density stratification using the eigenfunction expansion. Interestingly, for the channel case, the time-dependent diffusion-driven flow exhibits oscillations for some parameters and decays monotonically for other parameter combinations. This is different from the flows in the inclined plane problem, which always includes oscillating terms.

Second, the evolution of a passive scalar is crucial in numerous fields including microfluidics [3, 30], biology [22, 23], and oceanography[32]. Using the steady diffusion-driven flow solution, [37, 20] studied the optimal gap thickness and angle to maximize long time mixing of a passive scalar advected by a steady flow arising in the tilted parallel-plate channel domain. Intuitively, unsteady diffusion-driven flows generate different properties than their steady counterparts, while they are less studied in the literature, and investigating them is the second goal of this work. Using the time-dependent flow formula we derived, we calculate the effective diffusion coefficient of the passive scalar, which is a fundamental quantity to characterize the passive scalar distribution. Similar as in the steady case, the unsteady

2

diffusion-driven flow solution could significantly enhance the tracer dispersion. However, in some parameter regimes, the unsteady flow solution introduces considerably large oscillations in the effective diffusion coefficient and can even decrease the mixing coefficient temporally.

This paper is organized as follows. In section 2, we formulate the governing equation for the diffusion-driven flow and document the non-dimensionalization procedure. In section 3, we derive the expression of the diffusion-driven flow and the coupled density perturbation. In section 4, we study the effective diffusion coefficient of the passive scalar induced by the diffusion-driven flow and explore the optimal parameters for enhancing or reducing the effective diffusion coefficient.

2. Governing equation and nondimensionalization

2.1. Governing equation

There could be two different types of scalars in the system we consider: the stratifying scalar, C and a passive scalar T. The stratified scalar contributes to the density stratification, which creates diffusion-driven flows. The system could also include passive scalars, such as a fluorescent dye. The passive scalar will be passively advected by the fluid flow without changing the velocity field. Both scalars satisfy the advection-diffusion equation with no-flux boundary conditions, and the equation for the passive scalar takes the form

$$\partial_t T + \mathbf{u}(\mathbf{x}, t) \cdot \nabla T = \kappa_p \Delta T, \quad T(x, \mathbf{y}, 0) = T_I(x, \mathbf{y}), \quad \partial_{\mathbf{n}} T|_{boundary} = 0, \tag{1}$$

where κ_p is the passive scalar diffusivity, $T_I(x, \mathbf{y})$ is the initial data, $\mathbf{n}$ is the outward normal vector of the boundary. Figure 1 sketches two coordinate systems for a tilted parallel-plate channel domain with a inclination angle θ which satisfies $0 \leq \theta \leq \frac{\pi}{2}$. In this setup, x_3-direction is parallel to the direction of gravity, y_1-direction is the longitudinal direction of the channel. $\Omega = \{y_3 | y_3 \in [0, L]\}$ is the cross-section of the channel. The relation between the lab frame coordinates (x_1, x_2, x_3) and the coordinates (y_1, y_2, y_3) is

$$\begin{bmatrix} y_1 \\ y_3 \end{bmatrix} = \begin{bmatrix} \cos\theta & \sin\theta \\ -\sin\theta & \cos\theta \end{bmatrix} \begin{bmatrix} x_1 \\ x_3 \end{bmatrix}, \quad y_2 = x_2. \tag{2}$$

In (y_1, y_2, y_3) coordinates system, the direction of gravity is $(-\sin\theta, 0, -\cos\theta)$.

We assume the fluid density linearly depends on the stratified scalar. For example, the density of sodium chloride solution increases linearly as the concentration increases [18]. Therefore, the density field ρ and the fluid flow u_i satisfies the incompressible Navier-Stokes equation,

$$\rho\left(\partial_t u_i + \mathbf{u} \cdot \nabla u_i\right) = \mu \Delta u_i - \partial_{x_i} p - \rho g \delta_{i3}, \quad u_i|_{\partial\Omega} = 0, \quad i = 1, 2, 3, \quad \nabla \cdot \mathbf{u} = 0,$$
$$\partial_t \rho + \mathbf{u} \cdot \nabla \rho = \kappa_s \Delta \rho, \quad \partial_{\mathbf{n}} \rho|_{\partial\Omega} = 0, \quad \rho|_{|x_3| \to \infty} = \rho_0 - \Gamma x_3, \tag{3}$$

where δ_{ij} is the Kronecker delta, $g(cm/s^2)$ is the acceleration of gravity, Γ $(gram \cdot cm^{-4})$ is the density gradient, μ, $(gram \cdot cm^{-1} \cdot s^{-1})$ is the dynamic viscosity, p $(gram \cdot cm^{-1} \cdot s^{-2})$ is the pressure and κ_s (cm^2/s) is the molecular diffusivity of the stratified scalar. In this study, we make the assumption that the background density function varies linearly with height. This assumption is a local approximation to the scenario where the density function changes slowly with respect to height. By assuming this linearity, we aim to simplify the analysis while still capturing the essential behavior of the system.
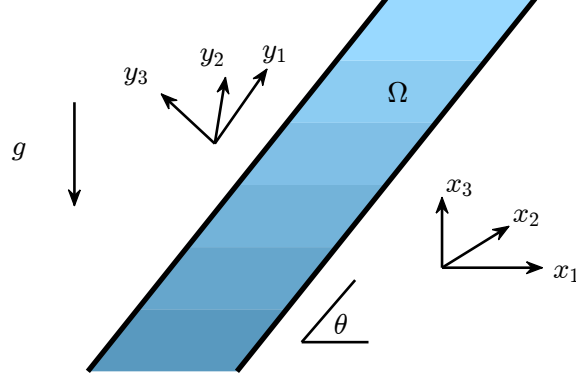
3

Figure 1: Schematic showing the setup for the diffusion-driven flow problem.

2.2. Nondimensionalization

Since we are interested in the dispersion of the passive scalar, we use the diffusion time scale of the passive scalar as the characteristic time scale of the whole system. With the change of variables

$$\rho_0 \rho' = \rho, \quad \frac{L^2}{\kappa_p} t' = t, \quad L x' = x, \quad U u' = u, \quad \frac{\mu U}{L} p' = p, \quad \kappa_p \kappa' = \kappa, \quad \frac{\rho_0}{L} \Gamma_0 = \Gamma,$$

$$T'(\mathbf{x}', t') L^{-3} \int_{\mathbb{R} \times \Omega} T_I(\mathbf{x}) \mathrm{d}\mathbf{x} = T(\mathbf{x}, t),$$

(4)

we have

$$\frac{\rho_0 U \kappa_p}{L^2} \rho' \partial_{t'} u_i' + \frac{\rho_0 U^2}{L} \rho' \mathbf{u}' \cdot \nabla_{\mathbf{x}'} u_i' = \frac{\mu U}{L^2} \Delta_{\mathbf{x}'} u_i' - \frac{\mu U}{L^2} \partial_{x_i'} p' - \rho_0 g \rho' \delta_{i3}, \ i = 1, 2, 3,$$

$$\frac{L^2}{\kappa_p} \partial_{t'} T' + \frac{U}{L} \mathbf{u} \nabla_{\mathbf{x}'} T' = \frac{\kappa_p}{L^2} \Delta_{\mathbf{x}'} T',$$

$$\frac{\rho_0 \kappa_p}{L^2} \partial_{t'} \rho' + \frac{U \tilde{\rho}}{L} \mathbf{u}' \cdot \nabla_{\mathbf{x}'} \rho' = \frac{\kappa_s \tilde{\rho}}{L^2} \Delta_{\mathbf{x}'} \rho'.$$

(5)

We can drop the primes without confusion and obtain the nondimensionalized version

$$\frac{\mathrm{Re}}{\mathrm{Pe_p}} \rho \partial_t u_i + \mathrm{Re} \rho \mathbf{u} \cdot \nabla u_i = \Delta u_i - \partial_{x_i} p - \frac{\mathrm{Re}}{\mathrm{Fr}^2} \rho \delta_{i3}, \quad i = 1, 2, 3,$$

$$\partial_t T + \mathrm{Pe}_p \mathbf{u} \cdot \nabla T = \Delta T,$$

$$\frac{1}{\kappa_2} \partial_t \rho + \mathrm{Pe}_s \mathbf{u} \cdot \nabla \rho = \Delta \rho,$$

(6)

where the non-dimensional parameters are the non-dimensionalized stratified scalar diffusivity $\kappa_2 = \frac{\kappa_s}{\kappa_p}$, Péclet number $\mathrm{Pe}_s = \frac{UL}{\kappa_s}$ and $\mathrm{Pe}_p = \frac{UL}{\kappa_p}$, Reynolds number $\mathrm{Re} = \frac{\rho_0 L U}{\mu}$, Froude number $\mathrm{Fr} = \frac{U}{\sqrt{gL}}$, and Schmidt number $\mathrm{Sc} = \frac{\mu}{\rho_0 \kappa_p} = \frac{\mathrm{Pe}_p}{\mathrm{Re}}$. If the scalar field is the temperature field, then κ_p is the thermal diffusivity and $\frac{\mu}{\rho_0 \kappa_p} = \frac{\mathrm{Pe}_p}{\mathrm{Re}}$ is the Prandtl number.

It is convenient to consider the problem in (y_1, y_2, y_3) coordinate system. We denote v_i as the velocity component along the y_i-direction. Since the initial condition and the boundary condition are independent of y_2, equation (1) and (6) becomes

$$\rho\left(\frac{1}{\mathrm{Sc}}\partial_t v_1 + \mathrm{Re}v_1\partial_{y_1}v_1 + \mathrm{Re}v_3\partial_{y_3}v_1\right) = \Delta v_1 - \partial_{y_1}p - \frac{\mathrm{Re}}{\mathrm{Fr}^2}\rho\sin\theta,$$

$$\rho\left(\frac{1}{\mathrm{Sc}}\partial_t v_3 + \mathrm{Re}v_1\partial_{y_1}v_3 + \mathrm{Re}v_3\partial_{y_3}v_3\right) = \Delta v_3 - \partial_{y_3}p - \frac{\mathrm{Re}}{\mathrm{Fr}^2}\rho\cos\theta, \tag{7}$$

$$\partial_t T + \mathrm{Pe}_p\mathbf{v}\cdot\nabla T = \Delta T,$$

$$\frac{1}{\kappa_2}\partial_t\rho + \mathrm{Pe}_s\mathbf{v}\cdot\nabla\rho = \Delta\rho, \quad \rho|_{|\mathbf{y}|\to\infty} = \rho_0 - \Gamma_0(y_1\sin\theta + y_3\cos\theta).$$

We next consider some combination of experimental physical parameters, which could give us the order of magnitude of the non-dimensional parameters and help with the perturbation analysis. The scaling relation for the characteristic velocity and the physical parameter varies for different boundary geometries. According to the formula in [28, 20], the characteristic velocity of steady diffusion-driven flow in the parallel-plate channel is $U = \kappa\left(\frac{g\Gamma}{\mu\kappa}\right)^{\frac{1}{4}}$ and the characteristic boundary layer thickness is $L_b = \left(\frac{g\Gamma}{\mu\kappa}\right)^{-\frac{1}{4}}$. In an experiment with sodium chloride solution, the parameters could be $g = 980$ cm/s^2, $\mu = 0.01$ gram/(cm.s), $\kappa_s = 1.5 \times 10^{-5}$ cm^2/s, $\Gamma = 0.007$ gram/cm^4, $\rho = 1$ gram/cm^3, we have $U = 0.00123353$ cm/s, $L_b = 0.0121602$ cm. If $L = 0.1$ cm, we have

$$\mathrm{Re} = 0.0123353, \quad \mathrm{Pe}_s = 8.22353, \quad \mathrm{Fr} = 0.000124605, \quad \mathrm{Sc} = 1000, \quad \frac{\mathrm{Re}}{\mathrm{Fr}^2} = 794468. \tag{8}$$

For a larger channel width $L = 1$ cm, we have

$$\mathrm{Re} = 0.123353, \quad \mathrm{Pe}_s = 82.2353, \quad \mathrm{Fr} = 0.0000394036, \quad \mathrm{Sc} = 1000, \quad \frac{\mathrm{Re}}{\mathrm{Fr}^2} = 7.94468 \times 10^7. \tag{9}$$

We can see that the Reynolds number is small, and the gravity term is important in the governing equation.

3. Flow equation

The Boussinesq approximation is commonly employed in the analysis of buoyancy-driven flow [11], as well as in previous studies of steady diffusion-driven flow [28, 39]. This approximation is valid when the relative change in density is small, i.e., $\partial_z\rho/\rho \ll 1$, which holds true for the above given parameters where the value is 0.007. Therefore, adopting the Boussinesq approximation is a reasonable choice. The Boussinesq approximation states that the density variation is only important in the buoyancy term,

$$\rho_0 \left(\frac{1}{\text{Sc}} \partial_t v_1 + \text{Re} v_1 \partial_{y_1} v_1 + \text{Re} v_3 \partial_{y_3} v_1 \right) = \Delta v_1 - \partial_{y_1} p - \frac{\text{Re}}{\text{Fr}^2} \rho \sin \theta,$$

$$\rho_0 \left(\frac{1}{\text{Sc}} \partial_t v_3 + \text{Re} v_1 \partial_{y_1} v_3 + \text{Re} v_3 \partial_{y_3} v_3 \right) = \Delta v_3 - \partial_{y_3} p - \frac{\text{Re}}{\text{Fr}^2} \rho \cos \theta,$$

$$\partial_t T + \text{Pe}_p \mathbf{v} \cdot \nabla T = \Delta T,$$

$$\frac{1}{\kappa_2} \partial_t \rho + \text{Pe}_s \mathbf{v} \cdot \nabla \rho = \Delta \rho, \quad \rho|_{|\mathbf{y}| \to \infty} = \rho_0 - \Gamma_0 (y_1 \sin \theta + y_3 \cos \theta). \tag{10}$$

Notice that, in this setup, the flow is invariant under the translation in y_1-direction. Hence, we can assume the velocity only depends on y_3. Then, the incompressibility $\partial_{y_1} v_1 + \partial_{y_3} v_3 = 0$ becomes $\partial_{y_3} v_2 = 0$ which implies $v_3 = 0$. To further simplify the equations, we introduce the density perturbation $f(y_3, t)$ which satisfies

$$\rho = \rho_0 + f(y_3, t) - \Gamma_0 (y_1 \sin \theta + y_3 \cos \theta). \tag{11}$$

We also write the pressure as $p = p_0 + \tilde{p}$, where p_0 balances the background density and solves the equation

$$\partial_{y_1} p_0 = -\frac{\text{Re}}{\text{Fr}^2} \sin \theta (\rho_0 - \Gamma_0 (y_1 \sin \theta + y_3 \cos \theta)),$$

$$\partial_{y_3} p_0 = -\frac{\text{Re}}{\text{Fr}^2} \cos \theta (\rho_0 - \Gamma_0 (y_1 \sin \theta + y_3 \cos \theta)). \tag{12}$$

Since the right hand side of the above equation is curl-free, the solution p_0 exists. In fact, we have

$$p_0 = -\frac{\text{Re}}{\text{Fr}^2} \left(\rho_0 y_3 \cos \theta + \rho_0 y_1 \sin \theta - \Gamma_0 y_1 y_3 \cos \theta \sin \theta - \frac{\Gamma_0}{2} y_3^2 \cos^2 \theta - \frac{\Gamma_0}{2} y_1^2 \sin^2 \theta \right). \tag{13}$$

Now, equation (10) becomes

$$\frac{1}{\text{Sc}} \rho_0 \partial_t v_1 = \partial_{y_3}^2 v_1 - \partial_{y_1} \tilde{p} - \frac{\text{Re}}{\text{Fr}^2} f \sin \theta, \quad v_1|_{y_3 = 0, 1} = 0, \quad v_1|_{t=0} = 0,$$

$$0 = -\partial_{y_3} \tilde{p} - \frac{\text{Re}}{\text{Fr}^2} f \cos \theta, \tag{14}$$

$$\frac{1}{\kappa_2} \partial_t f - \partial_{y_3}^2 f = \text{Pe}_s \Gamma_0 v_1 \sin \theta, \quad \partial_{y_3} f|_{y_3 = 0, 1} = \Gamma_0 \cos \theta, \quad f|_{t=0} = 0.$$

Obviously, $\tilde{p}$ can be a function of y_3 only. Due to the non-dimensionalization, $\rho_0 = 1$. We obtain the following equation for analyzing

$$\frac{1}{\text{Sc}} \partial_t v_1 - \partial_{y_3}^2 v_1 = -\frac{\text{Re}}{\text{Fr}^2} f \sin \theta, \quad v_1|_{y_3 = 0, 1} = 0, \quad v_1|_{t=0} = 0,$$

$$\frac{1}{\kappa_2} \partial_t f - \partial_{y_3}^2 f = \text{Pe}_s \Gamma_0 v_1 \sin \theta, \quad \partial_{y_3} f|_{y_3 = 0, 1} = \Gamma_0 \cos \theta, \quad f|_{t=0} = 0. \tag{15}$$
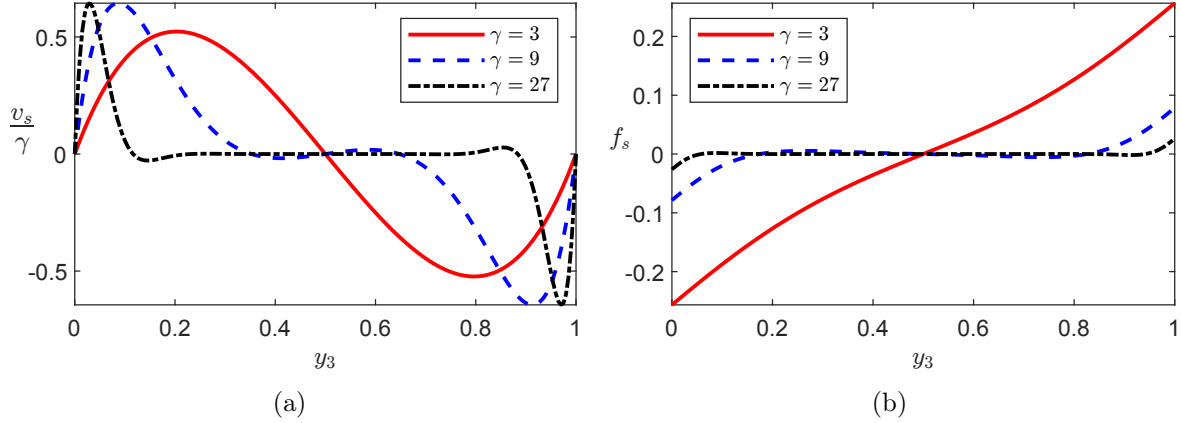
Figure 2: (a) Normalized steady flow solution $\frac{v_s}{\gamma}$ for various parameter γ. (b) The perturbed density field f_s for different γ.

We can decouple f and v_1 by differentiating the equation and obtain the following equations

$$\left(\frac{1}{\kappa_2}\partial_t - \partial_{y_3}^2\right)\left(\frac{1}{\mathrm{Sc}}\partial_t - \partial_{y_3}^2\right)v_1 = -\frac{\Gamma_0 \mathrm{RePe}_s\left(\sin\theta\right)^2}{\mathrm{Fr}^2}v_1, \quad v_1|_{y_3=0,1} = 0, \quad v_1|_{t=0} = 0,$$

$$\left(\frac{1}{\mathrm{Sc}}\partial_t - \partial_{y_3}^2\right)\left(\frac{1}{\kappa_2}\partial_t - \partial_{y_3}^2\right)f = -\frac{\Gamma_0 \mathrm{RePe}_s\left(\sin\theta\right)^2}{\mathrm{Fr}^2}f, \quad \partial_{y_3}f|_{y_3=0,1} = \Gamma_0\cos\theta, \quad f|_{t=0} = 0.$$

(16)

To focus on the transient dynamics, we decompose the density perturbation and velocity into the steady part and the transient part, namely, $f = f_s + f_t$, $v_1 = v_s + v_t$. We first consider the steady solution, which satisfies the following equation

$$\partial_{y_3}^4 v_s = -\frac{\mathrm{RePe}_s}{\mathrm{Fr}^2}\left(\sin\theta\right)^2\Gamma_0 v_s, \quad v_s|_{y_3=0,1} = 0, \quad \partial_{y_3}^3 v_s\big|_{y_3=0,1} = \frac{\mathrm{Re}}{\mathrm{Fr}^2}\Gamma_0\sin\theta\cos\theta,$$

$$\partial_{y_3}^4 f_s = -\frac{\mathrm{RePe}_s}{\mathrm{Fr}^2}\left(\sin\theta\right)^2\Gamma_0 f_s, \quad \partial_{y_3}f_s|_{y_3=0,1} = \Gamma_0\cos\theta, \quad \partial_{y_2}^2 f_s\big|_{y_3=0,1} = 0,$$

(17)

We can solve it easily and obtain the solution

$$f_s = \frac{\Gamma_0\cos\theta(\cos(\gamma(1-y_3))\cosh(\gamma y_3) - \cos(\gamma y_3)\cosh(\gamma(1-y_3)))}{\gamma(\sin(\gamma)+\sinh(\gamma))},$$

$$v_s = \frac{2\gamma\cot(\theta)}{\mathrm{Pe}_s}\frac{\sin(\gamma y_3)\sinh(\gamma(1-y_3)) - \sin(\gamma(1-y_3))\sinh(\gamma y_3)}{\sin(\gamma)+\sinh(\gamma)},$$

(18)

where $\gamma = \frac{1}{\sqrt{2}}\left(\frac{\mathrm{RePe}_s(\sin\theta)^2\Gamma_0}{\mathrm{Fr}^2}\right)^{\frac{1}{4}}$, which is consistent with the steady solution presented in [28, 20]. γ^{-1} indicates the thickness of the boundary layer. As shown in figure 2, both the flow and the perturbed density are confined in a narrow region near the boundary for a large γ. In addition, both f and v_1 are odd functions with respect to $y_3 = \frac{1}{2}$.

When the channel gap thickness approach to the infinity, the system should asymptoti-

cally converge to the case with the inclined plane. Indeed, as $\gamma \to \infty$, we have

$$
\begin{aligned}
f_s &= -\Gamma_0 \cos\theta \frac{e^{-\gamma y}\cos(\gamma y)}{\gamma}, \\
v_s &= \frac{2\gamma\cot(\theta)}{\mathrm{Pe}_s}\frac{e^{-\gamma y}\sin(\gamma y)}{2\gamma^3},
\end{aligned}
\tag{19}
$$

where is consistent with the solution presented in [28].

The transient part of the density perturbation f_t satisfies the equation

$$
\left(\left(\frac{1}{\mathrm{Sc}}\partial_t - \partial_{y_3}^2 \right)\left(\frac{1}{\kappa_2}\partial_t - \partial_{y_3}^2 \right) + \frac{\Gamma_0 \mathrm{RePe}_s\left(\sin\theta\right)^2}{\mathrm{Fr}^2} \right) f_t = 0,
\tag{20}
$$

$$
\partial_{y_2} f_t|_{y_3=0,1} = 0, \qquad f_t|_{t=0} = -f_s.
$$

We need one more condition to determine the solution. From $\left(\frac{1}{\kappa_2}\partial_t - \partial_{y_3}^2 \right) f = \mathrm{Pe}_s \Gamma_0 v_1 \sin\theta$,

we have $\left(\frac{1}{\kappa_2}\partial_t - \partial_{y_3}^2 \right) f\big|_{t=0} = 0$ which implies $\frac{1}{\kappa_2}\partial_t f_t\big|_{t=0} = \partial_{y_3}^2 f_t\big|_{t=0} + \partial_{y_3}^2 f_s = 0$. To shorten the expression, we denote $\phi_0 = 1$, $\lambda_0 = 0$ and $\phi_n = \sqrt{2}\cos n\pi y$, $\varphi_n = \sqrt{2}\sin n\pi y$, $\lambda_n = n^2\pi^2$, $n \ge 1$ as the eigenfunctions and eigenvalues of the Laplace operator in the cross section of the parallel-plate channel with no-flux boundary condition and pure absorbing boundary condition, respectively. To be more specific, $(\lambda_n - \Delta)\phi_n = 0$, $\partial_{y_3}\phi\big|_{y_3=0,1} = 0$ and $(\lambda_n - \Delta)\varphi_n = 0$, $\varphi\big|_{y_3=0,1} = 0$. Either $\{\phi_n\}_{n=0}^{\infty}$ or $\{\varphi_n\}_{n=1}^{\infty}\cup\{1\}$ form an orthogonal basis on the cross section Ω with respect to the inner product $\langle f(y_3), g(y_3) \rangle = \int_0^1 f(y_3)g(y_3)\mathrm{d}y_3$. For the velocity, we prefer to use φ_n, since the linear combination of them satisfies the boundary condition automatically. With the same argument, we prefer to use ϕ_n to represent the perturbed density field. The straightforward calculation yields

$$
f_t = -\sum_{n=1}^{\infty}\langle f_s, \phi_n \rangle \phi_n(y_3) e^{-\frac{1}{2}(\mathrm{Sc}+\kappa_2)\lambda_n t}\left(\cosh\left(\frac{a_n t}{2} \right) + \frac{\lambda_n\left(\mathrm{Sc}+\kappa_2\right)}{a_n}\sinh\left(\frac{a_n t}{2} \right) \right),
$$

$$
a_n = \sqrt{(\mathrm{Sc}-\kappa_2)^2\lambda_n^2 - 16\gamma^4 \mathrm{Sc}\kappa_2},
\tag{21}
$$

$$
\langle f_s, \phi_n \rangle = \frac{\sqrt{2}\Gamma_0\cos\theta\left((-1)^n - 1\right)\left(\sin(\gamma)\left(\pi^2 n^2 - 2\gamma^2\right) + \sinh(\gamma)\left(2\gamma^2 + \pi^2 n^2\right)\right)}{(4\gamma^4 + \pi^4 n^4)\left(\sin(\gamma) + \sinh(\gamma)\right)}.
$$

Then the cosine expansion of v_1 is available from the relation (15). We can obtain the sine expansion of the velocity using the same strategy. The transient part of the velocity component in y_1 direction satisfies the equation

$$
\left(\left(\frac{1}{\mathrm{Sc}}\partial_t - \partial_{y_3}^2 \right)\left(\frac{1}{\kappa_2}\partial_t - \partial_{y_3}^2 \right) + \frac{\Gamma_0 \mathrm{RePe}_s\left(\sin\theta\right)^2}{\mathrm{Fr}^2} \right) v_t = 0,
\tag{22}
$$

$$
v_t|_{y_3=0,1} = 0, \qquad v_t|_{t=0} = -v_s.
$$

We need one more condition to determine the solution. Based on $\left(\frac{1}{\mathrm{Sc}}\partial_t - \partial_{y_3}^2 \right) v_1 = -\frac{\mathrm{Pe}_2}{\mathrm{Fr}^2} f \sin\theta$, we have $\left(\frac{1}{\mathrm{Sc}}\partial_t - \partial_{y_3}^2 \right) v\big|_{t=0} = 0$ which implies $\frac{1}{\mathrm{Sc}}\partial_t v_t\big|_{t=0} = \partial_{y_3}^2 v_t\big|_{t=0} + \partial_{y_3}^2 v_s = 0$. We have

the series representation

$$v_t = -\sum_{n=1}^{\infty} \langle v_s, \varphi_n \rangle \, \varphi_n(y_3) e^{-\frac{1}{2}(\mathrm{Sc}+\kappa_2)\lambda_n t} \left(\cosh\left(\frac{a_n t}{2}\right) + \frac{\lambda_n \left(\mathrm{Sc}+\kappa_2\right)}{a_n} \sinh\left(\frac{a_n t}{2}\right) \right),$$

$$\langle v_s, \varphi_n \rangle = -\frac{2\gamma \cot(\theta)}{\mathrm{Pe}_s} \frac{2\sqrt{2}\pi\gamma^2 \left((-1)^n + 1\right) n(\cos(\gamma) - \cosh(\gamma))}{\left(4\gamma^4 + \pi^4 n^4\right)\left(\sin(\gamma) + \sinh(\gamma)\right)}.$$

(23)

In a system with the inclined plane, the transient part of the diffusion-driven flow decays algebraically and exhibits oscillation behavior for all Schmidt numbers [19]. Unlike the semi-infinite domain, here, the transient part of the flow vanishes exponentially. Moreover, v_t can be a monotonic function for some parameters and oscillatory for other parameter combinations. For instance, in the limiting case $\mathrm{Sc} = \infty$, we have

$$f_t = -\sum_{n=1}^{\infty} e^{-t\kappa_2\left(\frac{4\gamma^4}{\lambda_n} + \lambda_n\right)} \phi_n(y_3) \langle f_s, \phi_n \rangle,$$

$$v_t = -\sum_{n=1}^{\infty} e^{-t\kappa_2\left(\frac{4\gamma^4}{\lambda_n} + \lambda_n\right)} \varphi_n(y_3) \langle v_s, \varphi_n \rangle.$$

(24)

In this case, a_n is a real number for all n. Since $\langle v_s, \varphi_n \rangle$ is positive definite, $v_1 = v_s + v_t$ converges to the steady solution v_s monotonically.

When $\mathrm{Sc} = \kappa_2$, we have a simpler expression

$$f_t = -\sum_{n=1}^{\infty} \langle f_s, \phi_n \rangle \, \phi_n(y_3) e^{-\lambda_n \kappa_2 t} \left(\cos\left(2\gamma^2 \kappa_2 t\right) + \frac{\lambda_n}{2\gamma^2} \sin\left(2\gamma^2 \kappa_2 t\right) \right),$$

$$v_t = -\sum_{n=1}^{\infty} \langle v_s, \varphi_n \rangle \, \varphi_n(y_3) e^{-\lambda_n \kappa_2 t} \left(\cos\left(2\gamma^2 \kappa_2 t\right) + \frac{\lambda_n}{2\gamma^2} \sin\left(2\gamma^2 \kappa_2 t\right) \right).$$

(25)

In this case, a_n is a pure imaginary number for all n and the flow solution includes oscillatory terms. It is easy to show that the oscillation terms only appear if $a_n^2 < 0$ for some n, which can only happen when the parameters satisfy

$$\exists n \in \mathbb{Z}^+, \frac{\kappa_2 \left(8\gamma^4 - 4\sqrt{4\gamma^8 + \pi^4\gamma^4 n^4} + \pi^4 n^4\right)}{\pi^4 n^4} < \mathrm{Sc} < \frac{\kappa_2 \left(8\gamma^4 + 4\sqrt{4\gamma^8 + \pi^4\gamma^4 n^4} + \pi^4 n^4\right)}{\pi^4 n^4},$$

(26)

The inclined plane can be considered as a tilted parallel-plate channel domain with the infinite channel width. As the channel width L increases, Pe_2 and γ increases. For a large γ, we have the asymptotic expansion

$$\frac{\kappa_2 \left(8\gamma^4 - 4\sqrt{4\gamma^8 + \pi^4\gamma^4 n^4} + \pi^4 n^4\right)}{\pi^4 n^4} = \frac{\pi^4 n^4 \kappa_2}{16\gamma^4} + \mathcal{O}\left(\gamma^{-6}\right),$$

$$\frac{\kappa_2 \left(8\gamma^4 + 4\sqrt{4\gamma^8 + \pi^4\gamma^4 n^4} + \pi^4 n^4\right)}{\pi^4 n^4} = \frac{16\gamma^4 \kappa_2}{\pi^4 n^4} + 2\kappa_2 + \mathcal{O}\left(\gamma^{-1}\right).$$

(27)

9

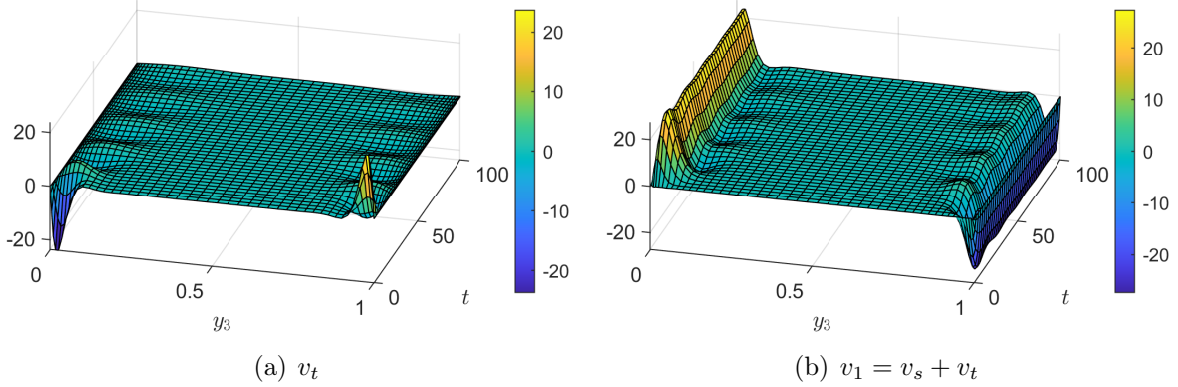(a) v_t (b) $v_1 = v_s + v_t$

Figure 3: Panel (a) The transient part of the diffusion-driven flow provided in equation (23). We use the terms with $n \leq 200$ in the series. We verify the truncation error is small enough by doubling the number of terms. Panel (b) The unsteady diffusion-driven flow solution. The parameters are $\text{Sc} = \kappa_2 = 10^{-4}$, $\gamma = 12\pi$, $\text{Pe}_s = 1$, $\theta = \frac{\pi}{4}$.

Therefore, in the large channel width limit, we observe the oscillation for all Sc, which is consistent with the conclusions for the inclined plane problem [19].

Next, we seek the parameters for observing pronounced oscillations in the time-dependent flow solution. The flow transient time scale (set by the longest lived mode) is $\frac{2}{(\text{Sc}+\kappa_2)\pi^2}$. The period of the associated oscillating term is $\frac{4\pi}{\sqrt{16\gamma^4 \text{Sc}\kappa_2 - (\text{Sc}-\kappa_2)^2\pi^4}}$. We are interested in maximizing the number of oscillations in this time interval which can be done by maximizing the ratio of these two time scales $\frac{2(\text{Sc}+\kappa_2)\pi^3}{\sqrt{16\gamma^4 \text{Sc}\kappa_2 - (\text{Sc}-\kappa_2)^2\pi^4}}$, which is the number of periods that we can observed within the transient time scale. In fact, when $\text{Sc} = \kappa_2$, this quantity reaches its maximum value $\frac{\gamma^2}{\pi^3}$. Figure 3 shows the evolution of the time-dependent diffusion-driven flow solution with $\text{Sc} = \kappa_2$. The transient part of the flow v_t is large near the boundary at a short time scale and then has oscillations with a relatively smaller amplitude. The oscillation amplitude is comparable to the magnitude of the steady solution. Therefore, from panel (b) of figure 3, we can see that the full flow solution has visible fluctuations. We remark that small values of Sc and κ_2 are possible if the stratified scalar is the temperature and the passive scalar is the salt solute, since the thermal diffusivity for liquid metals are generally of the order of 1 cm^2/s whereas the salt diffusivity is at the order of 10^{-5} cm^2/s.

Lastly, the original coupled equations for the velocity and perturbed density involve elliptic operators and first-order time derivatives, and at first glance, may appear similar to elliptic equations. However, the decoupled system (20) reveals a hyperbolic equation with a second-order time derivative, leading to distinct properties compared with elliptic equations. To illustrate the different, we compare equation (20) with the case of a second order diffusion problem with a Laplace-Beltrami operator using eigenfunction expansion with modes, $\phi_n(y)e^{-\lambda_n t}$. According to the Sturm-Liouville theory, the eigenfunction expansion has temporally decaying modes indexed by the well-ordered eigenvalues of a one-dimensional Laplace-Beltrami operator, $\lambda_n < \lambda_{n+1}$. For each mode, λ_n, the associated eigenfunction, $\phi_n(y)$ has exactly $n-1$ zeros, (notice that the higher dimensional results are different [5]). Interestingly, the operator in equation (20) doesn't have this property. For example, when

10

$\kappa_2 = 1$, $\gamma = 3$, $\mathrm{Sc} = \frac{1}{10}$, the coefficients of $\varphi_1(y_3) = \sqrt{2}\cos(\pi y_3)$ and $\varphi_2(y_3) = \sqrt{2}\cos(2\pi y_3)$ in equation (23) are, respectively,

$$
\langle v_s, \varphi_1 \rangle e^{-\frac{11\pi^2 t}{20}} \left(\frac{11\pi^2 \sin\left(\frac{1}{2}\sqrt{\frac{648}{5} - \frac{81\pi^4}{100}}\, t\right)}{10\sqrt{\frac{648}{5} - \frac{81\pi^4}{100}}} + \cos\left(\frac{1}{2}\sqrt{\frac{648}{5} - \frac{81\pi^4}{100}}\, t\right) \right),
$$

$$
\langle v_s, \varphi_2 \rangle e^{-\frac{11\pi^2 t}{5}} \left(\frac{22\pi^2 \sinh\left(\frac{1}{2}\sqrt{\frac{324\pi^4}{25} - \frac{648}{5}}\, t\right)}{5\sqrt{\frac{324\pi^4}{25} - \frac{648}{5}}} + \cosh\left(\frac{1}{2}\sqrt{\frac{324\pi^4}{25} - \frac{648}{5}}\, t\right) \right) \tag{28}
$$

$$
\sim \langle v_s, \varphi_2 \rangle \left(\frac{22\pi^2}{10\sqrt{\frac{324\pi^4}{25} - \frac{648}{5}}} + \frac{1}{2} \right) e^{\left(\frac{1}{2}\sqrt{\frac{324\pi^4}{25} - \frac{648}{5}} - \frac{11\pi^2}{5}\right)t}
$$

$$
+ \mathcal{O}\left(e^{-\left(\frac{1}{2}\sqrt{\frac{324\pi^4}{25} - \frac{648}{5}} + \frac{11\pi^2}{5}\right)t} \right), \quad t \to \infty.
$$

Since $-\frac{11\pi^2}{20} \approx -5.42828$ and $\frac{1}{2}\sqrt{\frac{324\pi^4}{25} - \frac{648}{5}} - \frac{11\pi^2}{5} \approx -4.88442$, the coefficient of φ_2 decays slower than the coefficient of φ_1 at long times, but has more spatial oscillations.

3.1. Quasi Boussinesq approximation

In the preceding section, we demonstrated how the Boussinesq approximation can simplify the problem and capture the nontrivial dynamics of the system, enabling us to obtain an exact solution for the unsteady shear flow. This approximation assumes a constant density function, denoted by ρ_0, in the time derivative term in equation (7). To further improve our understanding and capture more comprehensive behavior, we introduce an alternative approximation in this subsection that accounts for density variations in the y_3 direction, namely,

$$
(\rho_0 + f(y_3, t) - \Gamma_0 y_3 \cos\theta)\left(\frac{1}{\mathrm{Sc}}\partial_t v_1 + \mathrm{Re} v_1 \partial_{y_1} v_1 + \mathrm{Re} v_3 \partial_{y_3} v_1\right) = \Delta v_1 - \partial_{y_1} p - \frac{\mathrm{Re}}{\mathrm{Fr}^2}\rho\sin\theta,
$$

$$
(\rho_0 + f(y_3, t) - \Gamma_0 y_3 \cos\theta)\left(\frac{1}{\mathrm{Sc}}\partial_t v_3 + \mathrm{Re} v_1 \partial_{y_1} v_3 + \mathrm{Re} v_3 \partial_{y_3} v_3\right) = \Delta v_3 - \partial_{y_3} p - \frac{\mathrm{Re}}{\mathrm{Fr}^2}\rho\cos\theta,
$$

$$
\partial_t T + \mathrm{Pe}_p \mathbf{v} \cdot \nabla T = \Delta T,
$$

$$
\frac{1}{\kappa_2}\partial_t \rho + \mathrm{Pe}_s \mathbf{v} \cdot \nabla \rho = \Delta \rho, \quad \rho|_{|\mathbf{y}|\to\infty} = \rho_0 - \Gamma_0(y_1 \sin\theta + y_3 \cos\theta).
$$

$$
\tag{29}
$$

This is a valid approximation when $\theta \ll 1$, as $\rho \approx \rho_0 + f(y_3, t) - \Gamma_0 y_3 \cos\theta$. This approximation retains the most advantages of the Boussinesq approximation in analysis. First, we can still find the solution that only depends on y_3, resulting the following equation:

$$
\frac{1}{\mathrm{Sc}}\left(1 + f - \Gamma_0 y_3 \cos\theta\right)\partial_t v_1 - \partial_{y_3}^2 v_1 = -\frac{\mathrm{Re}}{\mathrm{Fr}^2} f \sin\theta, \quad v_1|_{y_3=0,1} = 0, \quad v_1|_{t=0} = 0,
$$

$$
\frac{1}{\kappa_2}\partial_t f - \partial_{y_3}^2 f = \mathrm{Pe}_s \Gamma_0 v_1 \sin\theta, \quad \partial_{y_3} f|_{y_3=0,1} = \Gamma_0 \cos\theta, \quad f|_{t=0} = 0.
$$

$$
\tag{30}
$$

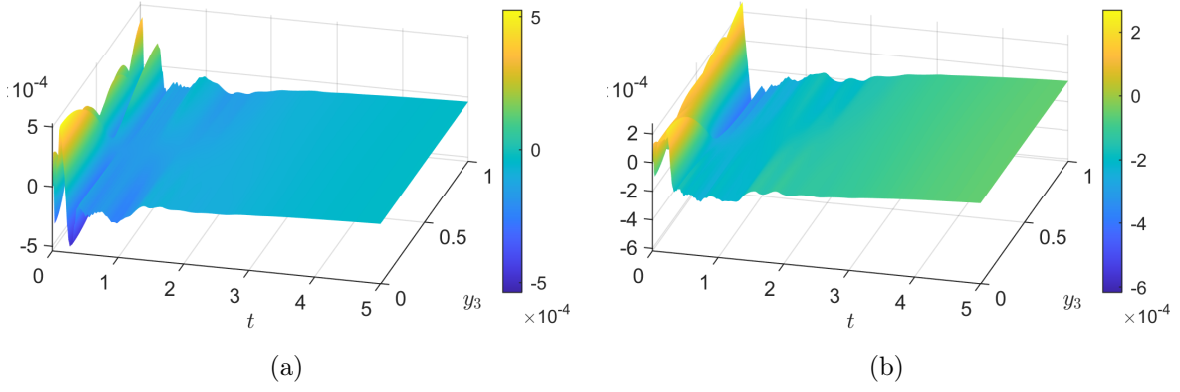(a)   (b)

Figure 4: The relative difference between the solution of equation (15) and the solution of equation (31) with $\theta = \frac{\pi}{4}$ in panel (a) and $\theta = \frac{\pi}{40}$ in panel (b). The rest parameters are $\gamma = 1$, $\Gamma_0 = 1$, $\kappa_2 = 1$, $Sc = 1$. The relative difference is defined as $\frac{f_1 - f_2}{max_{y_3,t}(f_1)}$, where f_1 denotes the solution of equation (15) and f_2 denotes the solution of equation (31)

Here, ρ_0 is set to 1 due to non-dimensionalization. Second, we can also decouple f and v_1 by differentiating the equation and obtain the following equation

$$\left(\frac{\frac{1}{Sc}(1 + f - \Gamma_0 y_3 \cos\theta)}{Sc} \partial_t - \partial_{y_3}^2 \right) \left(\frac{1}{\kappa_2} \partial_t - \partial_{y_3}^2 \right) f = -4\gamma^4 f,$$

$$\partial_{y_3} f|_{y_3=0,1} = \Gamma_0 \cos\theta, \quad f|_{t=0} = 0. \tag{31}$$

Once we have obtained the perturbed density field, we can use it to compute the velocity field with equation (30). The steady-state solutions of equations (15) under the Boussinesq approximation is the same as the solution of equation (30), but their transient dynamics differ. Due to the nonlinearity of the problem, it is difficult to find an exact analytical solution of equation (30), and here we numerically compute the solutions using `NDSolve` in Mathematica. We plot the relative difference between the solutions obtained from equations (15) and (30) in Figure 4. For both large and small inclination angles, the relative differences of the perturbed density field is around 10^{-4}, demonstrating that the system dynamics are not significantly affected by the transverse density variation in the time derivative term of the governing equation in this parameter regimes. This demonstrates the validity of the Boussinesq approximation for small angles.

4. Dispersion induced by the unsteady diffusion-driven flow

In this section, we focus on the evolution of passive scalar under the advection of the unsteady diffusion-driven flow. The well-known Taylor dispersion [31, 4] shows that as the flow acts to smear out the concentration distribution in the direction of the flow, it enhances the dispersion rate of the concentration distribution at which it spreads in that direction. Additionally, many approaches demonstrated that the distribution of a diffusing passive tracer under the shear flow advection is approximately governed by a diffusion equation with an effective diffusion coefficient at long-times, such as Hermite polynomial

12

series expansion [10], homogenization theory [38, 8], Aris moment approach [4, 34, 33, 12], center manifold theory [24, 36, 14] and the moment reconstruction [13, 6].

We first formulate the approximation theory of the Taylor dispersion. The reader can find more details in [14]. The effective equation for the governing equation of passive scalar (6) at long times is

$$\partial_t T + \text{Pe}_p \bar{v}_1 \partial_{y_1} T = \kappa_{\text{eff}}(t) \partial_{y_1}^2 T, \quad \kappa_{\text{eff}} = 1 + \text{Pe}_p \langle v_1 T_1 \rangle, \tag{32}$$

where T_1 is the solution of the auxiliary problem

$$\partial_t T_1 - \partial_{y_3}^2 T_1 = \text{Pe}_p (v_1 - \bar{v}_1), \quad T_1(y_3, 0) = 0, \quad \partial_{y_3} T_1 \big|_{y_3=0,1} = 0. \tag{33}$$

If the initial condition of the passive scalar is a Gaussian function $T\big|_{t=0} = \frac{1}{\sqrt{2\pi\sigma}} e^{-\frac{y_1^2}{2\sigma}}$, then we have the exact formula for the variance

$$\text{Var}(\bar{T})(t) = \text{Var}(\bar{T})(0) + 2 \int_0^t \kappa_{\text{eff}}(s) \mathrm{d}s. \tag{34}$$

For general initial conditions, we have more exponential decaying terms in the variance formula. Equation 34 is a valid approximation at long times. The exact variance formula can be found in [34, 33].

Using the relation between the flow and density perturbation (15), we have

$$\partial_t T_1 - \partial_{y_3}^2 T_1 = \text{Pe}_p \left(\frac{\frac{1}{\kappa_2} \partial_t f_t - \partial_{y_3}^2 f_t}{\text{Pe}_s \Gamma_0 \sin\theta} + v_s \right), \quad T_1(y_3, 0) = 0, \quad \partial_{y_3} T_1 \big|_{y_3=0,1} = 0. \tag{35}$$

The solution is

$$T_1 = \text{Pe}_p \sum_{n=1}^{\infty} \left(\frac{\langle f_s, \phi_n \rangle b_n}{\text{Pe}_s \Gamma_0 \sin\theta} + \langle v_s, \phi_n \rangle \left(\frac{1 - e^{-\lambda_n t}}{\lambda_n} \right) \right) \phi_n, \tag{36}$$

where

$$\langle v_s, \phi_n \rangle = -\frac{2\gamma \cot(\theta)}{\text{Pe}_s} \frac{\sqrt{2}\gamma \left((-1)^n - 1\right) \left(\sin(\gamma) \left(2\gamma^2 + \pi^2 n^2\right) + \sinh(\gamma) \left(2\gamma^2 - \pi^2 n^2\right)\right)}{\left(4\gamma^4 + \pi^4 n^4\right) \left(\sin(\gamma) + \sinh(\gamma)\right)},$$

$$b_n = \frac{-1}{\kappa_2 a_n \left(\lambda_n^2 (\kappa_2 + \text{Sc} - 2)^2 - a_n^2\right)} \left(e^{-t\lambda_n} \left(a_n^3 - a_n \lambda_n^2 \left(\text{Sc}^2 + \kappa_2 \left(-3\kappa_2 - 2\text{Sc} + 4\right)\right)\right) + \right.$$

$$e^{-\frac{\kappa_2 + \text{Sc}}{2} \lambda_n t} \left(a_n^3 \left(-\cosh\left(\frac{ta_n}{2}\right)\right)\right) - a_n^2 \lambda_n (3\kappa_2 + \text{Sc} - 2) \sinh\left(\frac{ta_n}{2}\right)$$

$$+ a_n \lambda_n^2 \left(\text{Sc}^2 + \kappa_2 \left(-3\kappa_2 - 2\text{Sc} + 4\right)\right) \cosh\left(\frac{ta_n}{2}\right)$$

$$\left. + \lambda_n^3 \left(\text{Sc} - \kappa_2\right) \left(\kappa_2 + \text{Sc} - 2\right) \left(\kappa_2 + \text{Sc}\right) \sinh\left(\frac{ta_n}{2}\right)\right)\right). \tag{37}$$

Then, we have the series representation of the effective diffusion coefficient

$$\kappa_{\text{eff}} = 1 + \text{Pe}_p^2 \sum_{n=1}^{\infty} \left(\frac{\langle f_s, \phi_n \rangle}{\text{Pe}_s \Gamma_0 \sin \theta} b_n + \langle v_s, \phi_n \rangle \left(\frac{1 - e^{-\lambda_n t}}{\lambda_n} \right) \right)$$

$$\times \left(\langle v_s, \phi_n \rangle - \frac{\langle f_s, \phi_n \rangle e^{-\frac{\kappa_2 + \text{Sc}}{2} \lambda_n t}}{\text{Pe}_s \Gamma_0 \sin \theta} \left(\sinh \left(\frac{t a_n}{2} \right) \frac{a_n^2 + \lambda_n^2 (\kappa_2^2 - \text{Sc}^2)}{2 \kappa_2 a_n} + \lambda_n \cosh \left(\frac{t a_n}{2} \right) \right) \right).$$

(38)

To understand the contribution from the transient part of the flow solution, we compare it with the effective diffusion coefficient induced by the steady flow solution,

$$\kappa_{\text{eff},s} = 1 + \text{Pe}_p^2 \sum_{n=1}^{\infty} \langle v_s, \phi_n \rangle^2 \left(\frac{1 - e^{-\lambda_n t}}{\lambda_n} \right),$$

(39)

and the long time limit of the effective diffusion coefficient

$$\kappa_{\text{eff}}(\infty) = 1 + \frac{\text{Pe}_p^2 \cot^2(\theta)}{2 \gamma \text{Pe}_2^2 (\sin(\gamma) + \sinh(\gamma))^2} \left(\frac{5}{2} \sin(2\gamma) + 6\gamma \sin(\gamma) \sinh(\gamma) + \right.$$

$$5 \cos(\gamma) \sinh(\gamma) + \gamma (\cosh(2\gamma) - \cos(2\gamma)) - 5 \cosh(\gamma)(\sin(\gamma) + \sinh(\gamma))).$$

(40)

As an example, in a realizable experiment of sodium fluorescein diffusing in stratified sodium chloride solution, the parameters could be $g = 980$ cm/s^2, $\mu = 0.01$ gram/(cm.s), $\Gamma = 0.007$ gram/cm^4, $\rho = 1$ gram/cm^3, $\theta = \frac{\pi}{4}$. The diffusivity of sodium fluorescein is $\kappa_2 = 4.2 \times 10^{-6}$ cm^2/s [9], and the diffusivity of sodium chloride is $\kappa_2 = 1.5 \times 10^{-5}$ cm^2/s [35]. Based on the formula of the effective diffusivity, we have $\kappa_{\text{eff}}(\infty) = 6.958$ for $L = 0.1$ cm, $\kappa_{\text{eff}}(\infty) = 13.103$ for $L = 1$ cm. The difference between the diffusivities of passive scalar and stratified scalar could be much larger in temperature stratified experiments, where the enhanced effective diffusivity will be more significant.

Panel (a) in figure 5 shows the effective diffusion coefficient induced by the unsteady flow present in figure 3, where the passive scalar molecular diffusivity is much smaller than the stratified scalar diffusivity. We can see that the effective diffusion coefficient induced by the steady flow converges to the limiting value at the passive scalar diffusion time scale $t = 1$, while the effective diffusion coefficient induced by the unsteady diffusion-driven flow persists huge oscillations with the amplitude that is around twice of the limiting value at relatively larger time scales. Panel (b) in figure 5 shows the effective diffusion coefficient when the molecular diffusivity of passive scalar and stratified scalar are same. In this case, the effective diffusion coefficients induced by the steady and unsteady flow solution are closer. Interestingly, instead of enhancing the effective diffusion coefficient, the unsteady flow solution temporally reduces the effective diffusion coefficient below 1. In contrast, the steady flow creates dispersion enhancement for all parameters, which can be easily verified from equation (39). Additionally, we emphasize this dispersion reducing phenomenon is not observed in the scalar transport with single-frequency time-varying periodic shear flows [34, 33, 12]. We think this reduction is due to the interaction of different modes in the space-time decomposition of the shear flow. In the appendix, we present a simple shear flow example that consists of two modes and can reduce the dynamic effective diffusion coefficient below 1 at the earlier stages of the evolution.
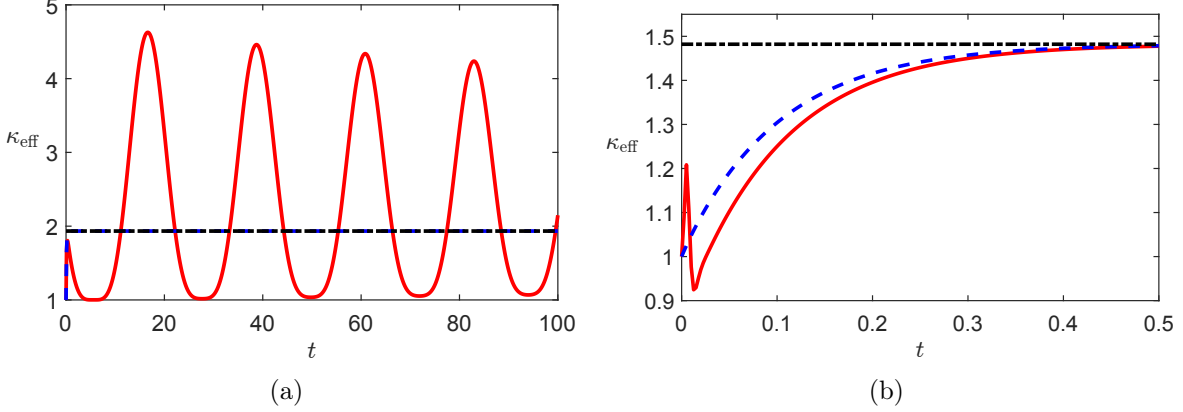
Figure 5: Effective diffusion coefficient for various parameters. The red solid line indicates the time dependent effective diffusion coefficient induced by the unsteady diffusion driven flow. The formula is provided in equation (38). The blue dashed line is the effective diffusion coefficient contributed by the steady part of the flow which is calculated by equation (39). The black dash-dot curve is the long time limit of the effective diffusion coefficient. The formula is provided in equation (40). Panel (a): The parameters are $Sc = \kappa_2 = 10^{-4}$, $\gamma = 12\pi$, $Pe_p = Pe_s = 1$, $\theta = \frac{\pi}{4}$. The corresponding velocity field is presented in figure 3. Panel (b): The parameters are $Sc = 50$, $\kappa_2 = 1$, $\gamma = 5$, $Pe_p = Pe_s = 1$, $\theta = \frac{\pi}{4}$.

To further understand this phenomenon, we are interested in the dependence of the minimum effective diffusion coefficient $\min_t \kappa_{\text{eff}}(t; Sc, \gamma)$ and the time for reaching its minimum value $t_{\min} = \text{argmin}_t \kappa_{\text{eff}}(t; Sc, \gamma)$ on Sc and γ. We numerically search the minimum value and the results are summarized in figure 6. We have several observations. First, in this parameter regime, as κ_2 decreases, $\min_{\gamma, Sc}(\min_t \kappa_{\text{eff}})$ decreases and $t_{\min}$ increases, which implies the dispersion reducing phenomenon is more significant for small κ_2, namely, when the passive scalar diffusivity is larger than the stratified scalar diffusivity. Second, $\min_t \kappa_{\text{eff}}(t; Sc, \gamma)$ is considerably less than 1 for moderate γ ($10 \sim 20$) and is closer to 1 for large γ.

Next, we focus on the dispersion enhancement at long times. First, we consider the dependence of the enhancement on the parameter γ. We have the asymptotic expansion of the effective diffusion coefficient for large and small γ,

$$
\begin{aligned}
\kappa_{\text{eff}}(\infty) &= 1 + \frac{Pe_p^2 \cot^2(\theta)}{Pe_s^2}\left(1 - \frac{5}{2\gamma} + \mathcal{O}(e^{-\gamma})\right), \quad \gamma \to \infty, \\
\kappa_{\text{eff}}(\infty) &= 1 + \frac{Pe_p^2 \cot^2(\theta)}{Pe_s^2}\left(\frac{\gamma^8}{22680} - \frac{2879\gamma^{12}}{4086482400} + O\left(\gamma^{13}\right)\right), \quad \gamma \to 0.
\end{aligned}
\tag{41}
$$

These asymptotic expansions suggest that the effective diffusion coefficient is bounded by $\frac{Pe_p^2 \cot^2(\theta)}{Pe_s^2} = \left(\frac{\kappa_2 \cot(\theta)}{\kappa_p}\right)^2$. In fact, $\gamma \to 0$ as the channel width L vanishes and $\gamma \to \infty$ as $L \to \infty$. When the channel width is small, the diffusion-driven flow is too weak to enhance the scalar dispersion. When the channel width is large, the diffusion-driven flow is confined in the region near the boundary and is not efficient to transport the scalar located far away from the boundary. Figure 7 shows the enhanced effective diffusion coefficient as a function of γ with $Pe_p = 1$. As we expected, the enhanced effective diffusion coefficient is zero when $\gamma = 0$, and converges to one as γ increases to infinity. This analysis shows that the
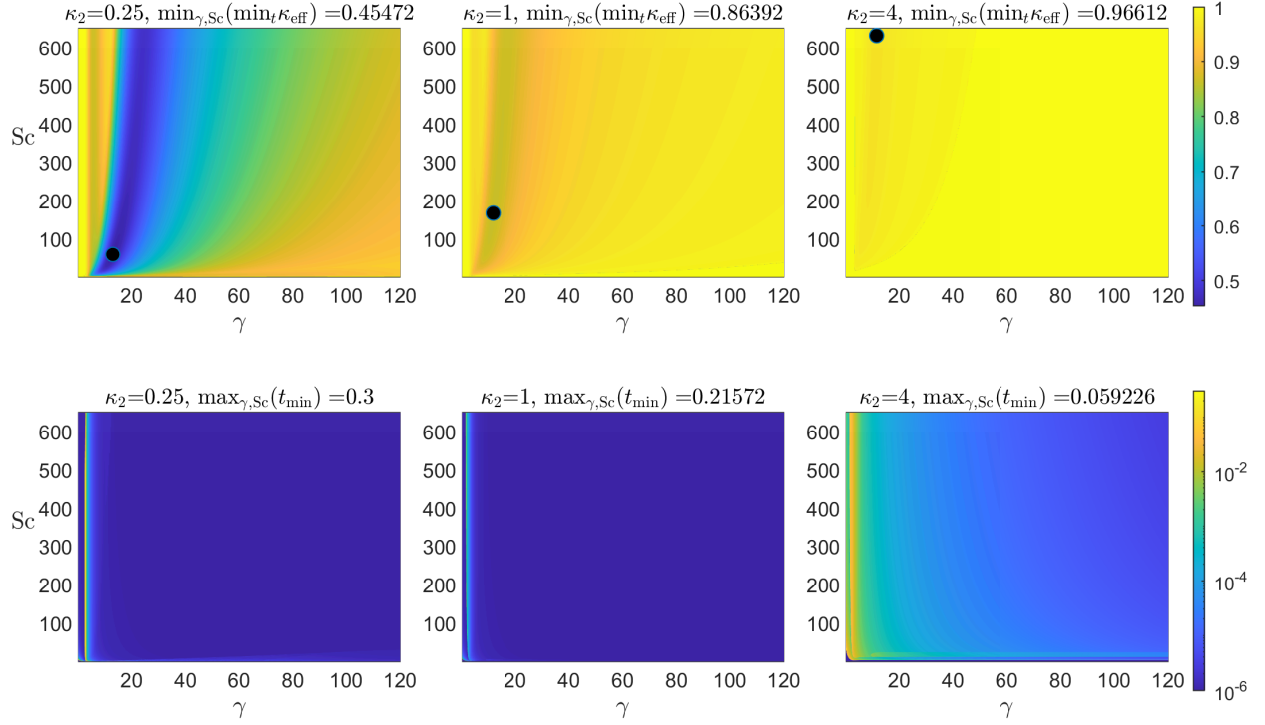
15

Figure 6: The first row shows the minimum value of the effective diffusion coefficient $\min_t \kappa_{\mathrm{eff}}(t)$ for $(\gamma, \mathrm{Sc}) \in (0, 120] \times (0, 400]$, three different κ_2, $\theta = \frac{\pi}{4}$ and $\mathrm{Pe}_p = \mathrm{Pe}_s = 1$. The black dot indicates the location of the minimum value $\min_{\gamma, \mathrm{Sc}} (\min_t \kappa_{\mathrm{eff}})$ in this parameter regime. The optimal parameters for reaching $\min_{\gamma, \mathrm{Sc}} (\min_t \kappa_{\mathrm{eff}})$ are $\gamma = 12.9407$ and $\mathrm{Sc} = 58.5349$ for $\kappa_2 = 0.25$, $\gamma = 11.6999$ and $\mathrm{Sc} = 166.6348$ for $\kappa_2 = 1$, $\gamma = 10.16$ and $\mathrm{Sc} = 400$ for $\kappa_2 = 4$. The second row shows $t_{\min}$ for κ_{eff} reaching the minimum value. We use the terms with $n \leq 259$ in the series.
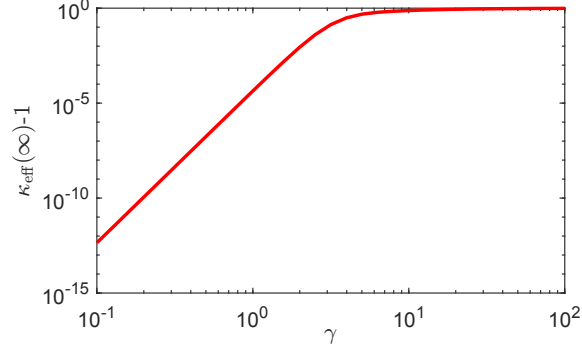
16

Figure 7: $\kappa_{\mathrm{eff}} - 1$ against the nondimensional parameter $\gamma = \frac{1}{\sqrt{2}} \left(\frac{\mathrm{Re}\,\mathrm{Pe}_s (\sin\theta)^2 \Gamma_0}{\mathrm{Fr}^2} \right)^{\frac{1}{4}}$. The parameters are $\mathrm{Pe}_p = \mathrm{Pe}_s = 1$ and $\theta = \frac{\pi}{4}$.
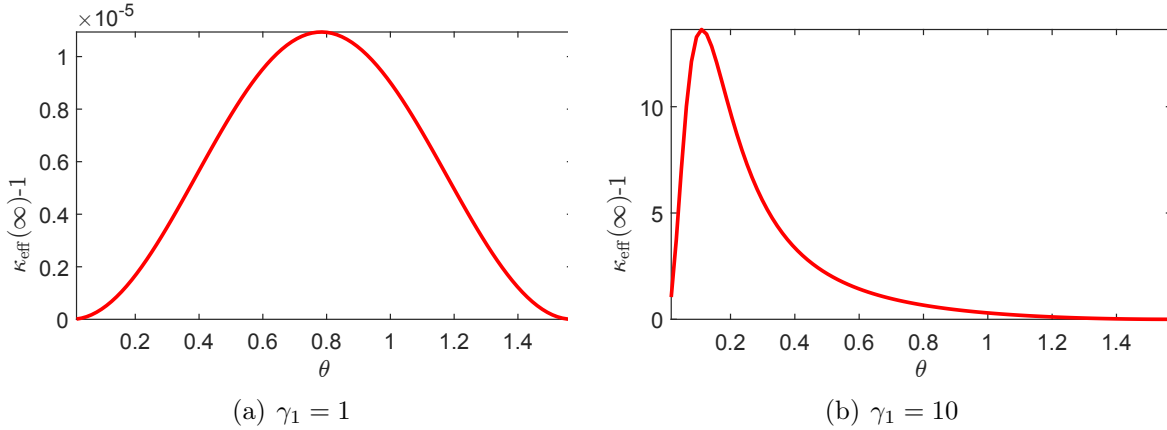

(a) $\gamma_1 = 1$

(b) $\gamma_1 = 10$

Figure 8: $\kappa_{\mathrm{eff}} - 1$ against the inclination angle θ. The parameters are $\mathrm{Pe}_p = \mathrm{Pe}_s = 1$. In panel (a), $\gamma_1 = 1$, in panel (b) $\gamma_1 = 10$.

dispersion of the stratified scalar can at most be doubled in the presence of diffusion-driven flow. In contrast, the effective diffusion coefficient of the passive scalar could be significantly enhanced by the diffusion-driven flow when the passive scalar diffusivity κ_p is much smaller than the stratified scalar diffusivity κ_s, namely, $\mathrm{Pe}_p \gg \mathrm{Pe}_s$.

Second, we consider the dependence of effective diffusion coefficient on two different Péclet numbers. The shear flow enhanced effective diffusion coefficient of a passive scalar is proportional to the square of the Péclet number Pe_p, which has been demonstrated by many methods such as homogenization theory [38, 8], Aris moment approach [4, 34, 33, 12]. All formulae of the effective diffusion coefficient (38), (39) and (40) are consistent with this conclusion. In contrast, the effective diffusion has a much more complicated dependence upon the stratified scalar's Peclet number, Pe_s, as is clear from the formula given in (40).

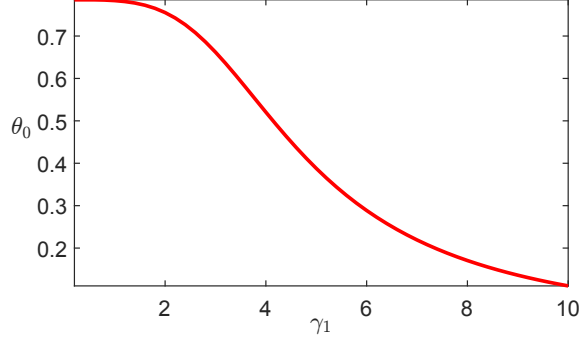Third, we study the dependence of the effective diffusion coefficient on the inclination

Figure 9: The optimal inclination angle θ_0 for inducing the maximum effective diffusion coefficient as a function of the parameter $\gamma_1 = \frac{1}{\sqrt{2}} \left(\frac{\text{RePe}_s \Gamma_0}{\text{Fr}^2} \right)^{\frac{1}{4}}$. The parameters are $\text{Pe}_p = \text{Pe}_s = 1$.

angle. For fixed Péclet numbers and $\gamma_1 = \frac{1}{\sqrt{2}} \left(\frac{\text{RePe}_s \Gamma_0}{\text{Fr}^2} \right)^{\frac{1}{4}}$, we have

$$\kappa_{\text{eff}}(\infty) = 1 + \frac{\text{Pe}_p^2}{\text{Pe}_s^2} \left(\frac{\gamma_1^8 \theta^2}{22680} + \mathcal{O}\left(\theta^{5/2}\right) \right), \quad \theta \to 0,$$

$$\kappa_{\text{eff}}(\infty) = 1 + \frac{\text{Pe}_p^2 \left(\theta - \frac{\pi}{2}\right)^2}{2\gamma_1 \text{Pe}_s^2} \left(\frac{5}{2} \sin(2\gamma_1) + 5\cos(\gamma_1)\sinh(\gamma_1) - 5\cosh(\gamma_1)(\sin(\gamma_1) + \sinh(\gamma_1)) \right)$$

$$6\gamma_1 \sin(\gamma_1) \sinh(\gamma_1) + \gamma_1 + (\cosh(2\gamma_1) - \cos(2\gamma_1))) + \mathcal{O}\left(\theta - \frac{\pi}{2}\right)^3, \quad \theta \to \frac{\pi}{2}. \tag{42}$$

Figure 8 plots the enhanced effective diffusion coefficient as a function of the inclination angle θ. The enhanced effective diffusion coefficient vanishes at $\theta = 0$ and $\frac{\pi}{2}$, which is consistent with the asymptotic expansions (41). The shape of this curve depends on the value of γ_1. It is symmetric when γ_1 is small, and skewed when γ_1 is large. Numerical calculation shows that the enhanced effective diffusion coefficient reaches the maximum value $\kappa_{\text{eff}} \approx 0.0000109356$ at $\theta \approx 0.783409 < \frac{\pi}{4}$ when $\gamma_1 = 1$, and reaches the maximum value $\kappa_{\text{eff}} \approx 13.6319$ at $\theta \approx 0.110802$ when $\gamma_1 = 10$. Figure 9 shows the optimal inclination angle θ_0 for inducing the maximum effective diffusion coefficient as a function of the parameter γ_1. For small γ_1, the optimal inclination angle is around $\theta = \frac{\pi}{4} \approx 0.785398$ which can be seen from equation (41). As γ_1 increases, the optimal inclination angle decreases. The dependence of the enhanced effective diffusion coefficient on the inclination angle and the parameter γ_1 is summarized in figure 10.

5. Conclusion and discussion

Here we have explored the diffusion-driven flow in the tilted parallel-plate channel domain with a linear density stratification along with the effective mixing of a diffusing passive scalar advected by this flow. Exact expressions for the flow were derived using an eigenfunction expansion, where it was established that the unsteady flow converges to the steady solution monotonically or oscillatory depending on the relation between the Schmidt number and the non-dimensionalized diffusivity. We demonstrated that when $\kappa_2 = \text{Sc}$, we have the most observable oscillations in the flow evolution. We then calculated the exact scalar
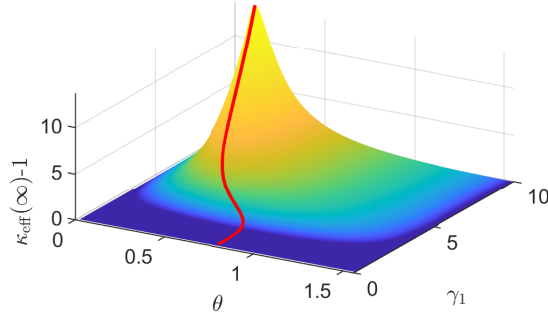
18

Figure 10: The enhanced effective diffusion coefficient as a function of the inclination angle and the parameter γ_1. The red solid line indicates the optimal inclination angle θ_0 for inducing the maximum effective diffusion coefficient when the parameter $\gamma_1 = \frac{1}{\sqrt{2}} \left(\frac{\mathrm{RePe}_s\Gamma_0}{\mathrm{Fr}^2} \right)^{\frac{1}{4}}$ is given. The parameters are $\mathrm{Pe}_p = \mathrm{Pe}_s = 1$.

distribution variance evolution and effective diffusion coefficient for the passive scalar. The formula demonstrates that the diffusion-driven flow could significantly enhance the effective diffusion coefficient of the scalar, especially when the molecular diffusivity of the passive scalar is much smaller than the stratified scalar diffusivity. This enhancement could have potential applications in geophysics and in microfluidics. We discovered a nonlinear dependence between the enhanced effective diffusion coefficient and the Péclet number of the stratified scalar, which is different from the typical quadratic scaling relation for the passive scalar in a shear flow.

Future work includes several directions. First, the steady diffusion-driven flow has been studied in many different boundary geometries [17, 27, 26, 16]. We are interested in investigating the time-dependent solution in those domains. Second, the current analysis assumes a linear stratification to simplify the calculation. In future work, we are interested in analyzing the flow and scalar evolution using full numerical simulations to further explore the validity of the Boussinesq approximation. Third, the diffusion-driven flow might exist in the presence of other external force fields as long as the direction of the external force field is not parallel to the impermeable boundary. One possible external force field is the electric field, and therefore we expect the diffusion-driven flow could be observed in some electrohydrodynamic problems.

6. Acknowledgements

Appendix A. Reduction of the effective diffusion coefficient

We present a simple shear flow that explicitly demonstrates a case in which the dynamic effective coefficient can be less than one on transient timescales. When $v(y,t) = \sqrt{2}\cos\pi y \left(e^{-2t} - e^{-t} \right)$, the solution of equation (33) is

$$T_1 = \frac{e^{-\pi^2 t} \left(e^{(\pi^2-2)t} \left((\pi^2 - 2)(-e^t) + \pi^2 - 1 \right) - 1 \right)}{2 - 3\pi^2 + \pi^4}, \tag{A.1}$$

19

The effective diffusion coefficient is given by

$$\kappa_{\text{eff}}(t) = 1 - \text{Pe}_p^2 \frac{e^{-\left(2+\pi^2\right)t}\left(e^t - 1\right)\left(e^{\left(\pi^2-2\right)t}\left(\left(\pi^2 - 2\right)e^t + \pi^2 - 1\right) - 2\pi^2 + 3\right)}{2 - 3\pi^2 + \pi^4}. \qquad (A.2)$$

When $\text{Pe}_p = 1$, $\kappa_{\text{eff}}(1) \approx 0.986359 < 1$, namely, the longitudinal dispersion is temporally reduced by this time-dependent shear flow.

References

[1] Allshouse, M.R., 2010. Novel applications of diffusion-driven flow. Ph.D. thesis. Massachusetts Institute of Technology.

[2] Allshouse, M.R., Barad, M.F., Peacock, T., 2010. Propulsion generated by diffusion-driven flow. Nature Physics 6, 516–519.

[3] Aminian, M., Bernardi, F., Camassa, R., Harris, D.M., McLaughlin, R.M., 2016. How boundaries shape chemical delivery in microfluidics. Science 354, 1252–1256.

[4] Aris, R., 1956. On the dispersion of a solute in a fluid flowing through a tube. Proceedings of the Royal Society of London. Series A. Mathematical and Physical Sciences 235, 67–77.

[5] Berkolaiko, G., Canzani, Y., Cox, G., Marzuola, J.L., 2022. Stability of spectral partitions and the dirichlet-to-neumann map. arXiv preprint arXiv:2201.00773 .

[6] Camassa, R., Ding, L., Kilic, Z., McLaughlin, R.M., 2021. Persisting asymmetry in the probability distribution function for a random advection-diffusion equation in impermeable channels. Physica D: Nonlinear Phenomena , 132930doi:`https://doi.org/10.1016/j.physd.2021.132930`.

[7] Camassa, R., Harris, D.M., Hunt, R., Kilic, Z., McLaughlin, R.M., 2019. A first-principle mechanism for particulate aggregation and self-assembly in stratified fluids. Nature communications 10, 1–8.

[8] Camassa, R., Lin, Z., McLaughlin, R.M., 2010. The exact evolution of the scalar variance in pipe and channel flow. Communications in Mathematical Sciences 8, 601–626.

[9] Casalini, T., Salvalaglio, M., Perale, G., Masi, M., Cavallotti, C., 2011. Diffusion and aggregation of sodium fluorescein in aqueous solutions. The Journal of Physical Chemistry B 115, 12896–12904.

[10] Chatwin, P., 1970. The approach to normality of the concentration distribution of a solute in a solvent flowing along a straight pipe. Journal of Fluid Mechanics 43, 321–352.

[11] Deen, W.M., 1998. Analysis of transport phenomena. volume 2. Oxford university press New York.

[12] Ding, L., Hunt, R., McLaughlin, R.M., Woodie, H., 2021. Enhanced diffusivity and skewness of a diffusing tracer in the presence of an oscillating wall. Research in the Mathematical Sciences 8, 1–29. doi:https://doi.org/10.1007/s40687-021-00257-4.

[13] Ding, L., McLaughlin, R.M., 2021. Ergodicity and invariant measures for a diffusing passive scalar advected by a random channel shear flow and the connection between the Kraichnan-Majda model and Taylor-Aris dispersion. Physica D: Nonlinear Phenomena , 133118doi:https://doi.org/10.1016/j.physd.2021.133118.

[14] Ding, L., McLaughlin, R.M., 2022. Determinism and invariant measures for diffusing passive scalars advected by unsteady random shear flows. Physical Review Fluids 7, 074502. doi:https://10.1103/PhysRevFluids.7.074502.

[15] Dressaire, E., Yamada, L., Song, B., Roper, M., 2016. Mushrooms use convectively created airflows to disperse their spores. Proceedings of the National Academy of Sciences 113, 2833–2838.

[16] French, A., 2017. Diffusion-driven flow in three dimensions. Ph.D. thesis. Monash University.

[17] Grayer, H., Yalim, J., Welfert, B.D., Lopez, J.M., 2020. Dynamics in a stably stratified tilted square cavity. Journal of Fluid Mechanics 883.

[18] Hall, R.E., 1924. The densities and specific volumes of sodium chloride solutions at 25°. Journal of the Washington Academy of Sciences 14, 167–173.

[19] Harabin, G., 2016. Diffusively Driven Shear Flows in Stratified Fluids. Ph.D. thesis. The University of North Carolina at Chapel Hill.

[20] Heitz, R., Peacock, T., Stocker, R., 2005. Optimizing diffusion-driven flow in a fissure. Physics of Fluids 17, 128104.

[21] Kistovich, A., Chashechkin, Y.D., 1993. The structure of transient boundary flow along an inclined plane in a continuously stratified medium. Journal of Applied Mathematics and Mechanics 57, 633–639.

[22] Lin, Z., Thiffeault, J.L., Childress, S., 2011. Stirring by squirmers. Journal of Fluid Mechanics 669, 167–177.

[23] Lin, Z., Zhu, S., Ding, L., 2022. Stirring by anisotropic squirming. Theoretical and Applied Mechanics Letters , 100358doi:https://doi.org/10.1016/j.taml.2022.100358.

[24] Mercer, G., Roberts, A., 1990. A centre manifold description of contaminant dispersion in channels with varying flow properties. SIAM Journal on Applied Mathematics 50, 1547–1565.

[25] Mercier, M.J., Ardekani, A.M., Allshouse, M.R., Doyle, B., Peacock, T., 2014. Self-propulsion of immersed objects via natural convection. Physical review letters 112, 204501.

[26] Page, M.A., 2011a. Combined diffusion-driven and convective flow in a tilted square container. Physics of Fluids 23, 056602.

[27] Page, M.A., 2011b. Steady diffusion-driven flow in a tilted square container. The Quarterly Journal of Mechanics & Applied Mathematics 64, 319–348.

[28] Phillips, O., 1970. On flows induced by diffusion in a stably stratified fluid, in: Deep Sea Research and Oceanographic Abstracts, Elsevier. pp. 435–443.

[29] Shaughnessy, E.J., Van Gilder, J.W., 1995. Low rayleigh number conjugate convection in straight inclined fractures in rock. Numerical Heat Transfer, Part A: Applications 28, 389–408.

[30] Stroock, A.D., Dertinger, S.K., Ajdari, A., Mezic, I., Stone, H.A., Whitesides, G.M., 2002. Chaotic mixer for microchannels. Science 295, 647–651.

[31] Taylor, G.I., 1953. Dispersion of soluble matter in solvent flowing slowly through a tube. Proceedings of the Royal Society of London. Series A. Mathematical and Physical Sciences 219, 186–203.

[32] Thomas, J., Gupta, A., 2022. Wave-enhanced tracer dispersion. Journal of Geophysical Research: Oceans 127, e2020JC017005.

[33] Vedel, S., Bruus, H., 2012. Transient Taylor–Aris dispersion for time-dependent flows in straight channels. Journal of fluid mechanics 691, 95–122.

[34] Vedel, S., Hovad, E., Bruus, H., 2014. Time-dependent Taylor–Aris dispersion of an initial point concentration. Journal of fluid mechanics 752, 107–122.

[35] Vitagliano, V., Lyons, P.A., 1956. Diffusion coefficients for aqueous solutions of sodium chloride and barium chloride. Journal of the American Chemical Society 78, 1549–1552.

[36] Wang, W., Roberts, A.J., 2013. Self-similarity and attraction in stochastic nonlinear reaction-diffusion systems. SIAM Journal on Applied Dynamical Systems 12, 450–486.

[37] Woods, A.W., Linz, S.J., 1992. Natural convection and dispersion in a tilted fracture. Journal of Fluid Mechanics 241, 59–74.

[38] Wu, Z., Chen, G., 2014. Approach to transverse uniformity of concentration distribution of a solute in a solvent flowing along a straight pipe. Journal of Fluid Mechanics 740, 196–213.

[39] Wunsch, C., 1970. On oceanic boundary mixing, in: Deep Sea Research and Oceanographic Abstracts, Elsevier. pp. 293–301.

[40] Zagumennyi, I.V., Dimitrieva, N., 2016. Diffusion induced flow on a wedge-shaped obstacle. Physica Scripta 91, 084002.